Channel Capacity of High Altitude Platform Systems employing Non-Coherent Detection

Dung lượng kênh cho hạ tầng truyền thông trên cao sử dụng tách sóng không nhất quán

Nguyen Thu Hien*, Nguyen Viet Hung, Vu Van San

Posts and Telecommunications Institute of Technology, Km 10, Nguyen Trai, Ha Dong, Hanoi, Viet Nam

Received: December 27, 2016; accepted: September 5, 2017

Abstract

In this paper, we present the results of calculating the Differential Discrete-input Continuous-output Memoryless Channel (D-DCMC) capacity for the High Altitude Platform (HAP) systems using extrinsic information transfer (EXIT) chart tool. Influencing factors of the propagation environment such as free space loss, attenuation due to meteorological effects, and multipath fading are also taken into consideration in modelling HAP transmission channel. Furthermore, in order to benchmark the near-capacity channel code design, we compute the outage capacity of D-DCMC for HAP systems.

Keywords: High altitude platform, non-coherent detection, differential discrete-input continuous-output memoryless channel, channel capacity, outage capacity.

Tóm tắt

Trong bài báo này, chúng tôi trình bày các kết quả tính toán dung lượng kênh không nhớ đầu vào rời rạc đầu ra liên tục vi sai (D-DCMC) cho hệ thống hạ tầng truyền thông trên cao (HAP) sử dụng công cụ biểu đồ truyền đạt thông tin ngoại lai (EXIT). Những yếu tố ảnh hưởng của môi trường truyền lan như suy hao không gian tự do, suy hao do ảnh hưởng của khí tượng, và pha-đinh đa đường cũng được xem xét trong mô hình hóa kênh truyền HAP. Hơn nữa, để đánh giá thiết kế mã kênh tiếp cận dung lượng, chúng tôi thực hiện tính toán dung lượng tới hạn của kênh D-DCMC cho hệ thống HAP.

Từ khóa: Hạ tầng truyền thông trên cao, tách sóng không nhất quán, kênh không nhớ đầu vào rời rạc đầu ra liên tục, dung lượng kênh, dung lượng tới hạn.

1. Introduction

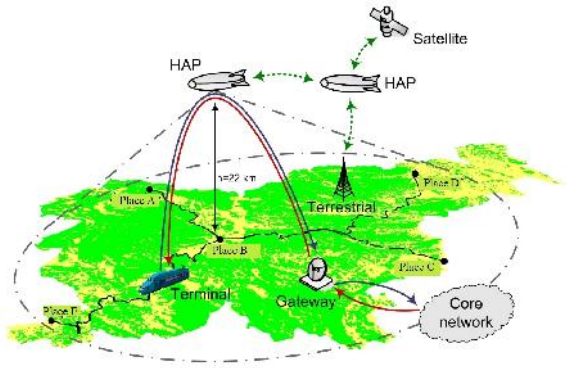

Fig. 1. Communication scenario in HAP.

Ubiquitous connectivity is considered a driving factor towards economic growth as no citizen is excluded from the benefits of broadband communications. However, to achieve global connectivity, heterogeneous network topologies must be efficiently deployed and interconnect with each other. To this end, High Altitude Platforms (HAPs) represent an efficacious alternative infrastructure and play an intermediate role by interconnecting terrestrial networks [1] (Fig. 1). HAPs, when fully deployed will have the capability of providing services and applications ranging from broadband wireless access, navigation and positioning systems, remote sensing and weather observation/monitoring systems, future generation mobile telephony, digital TV, etc. [2].

In Fig. 1, HAPs are communication facilities situated at an altitude of 17 to 30 km and at a specified fixed point relative to the Earth. They are mostly solar-powered, unmanned, and remotely operated [2]. Services can be provided from a single HAP with up-and down-links to the user terminals, together with backhaul links as required into the fiber backbone. Inter-HAP links may serve to connect a network of HAPs [2]. Fig. 1 also shows an example of the infrastructure required in a HAP communication system that consists of stratospheric stations, ground stations equipped for telecommunications and flight control, as well as fixed/mobile subscriber stations used for narrow/broadband services [2].

* Corresponding author: Tel.: (+84) 902.002.030
Email: hiennt@ptit.edu.vn

Although, HAPs preserve some of the best characteristics of terrestrial and satellite communication systems, while avoiding many of their drawbacks. HAP is not intended to replace these existing technologies, but instead to work with them in a complementary and integrated fashion [2]. The important benefit of HAP is its capability to deliver a high transmission capacity that is similar to that available from terrestrial systems along with providing a wide coverage similar to that available from satellite systems. Only recently project Loon has been revealed by Google utilizing solar-powered stratospheric balloons that are fully equipped with transceivers offering Internet connectivity to areas which lack broadband infrastructure [3].

In the design of wireless systems in general and HAP systems in particular, the selection of a coherent or non-coherent detection should be carefully considered. Coherent detection implies that the receiver must know the carrier phase, and this information obtain through synchronization. Tracking the received radio frequency signal phase require additional hardware (i.e., using phase lock loop), and implies higher power consumption. Non-coherent detection is simpler and can consume less power because it does not require a local oscillator. Many of the systems operating today have coherent receivers. Because it is generally thought that the performance of coherent is superior to non-coherent in a typical additive white Gaussian noise environment [4].

However, real environments for wireless communications as well as HAP are affected by fluctuations in amplitude and phase due to a frequency selective fading channel or phase noise caused by frequency oscillators, the non-coherent option could be a better option for designers. In addition, non-coherent detection is attractive when the carrier recovery circuit needed for coherent detection is difficult to implement, as is the case for high frequency signals such as microwaves and millimeter wave, or when the time delay associated with carrier synchronization reduces the system throughput to less than the minimum needed for Quality of Service (QoS) [5].

Extrinsic Information Transfer (EXIT) charts [6] constitute an excellent tool designed for analyzing the convergence behavior of an iterative decoding/detection scheme without performing time-consuming bit-by-bit decoding. Symbol based EXIT charts of non-binary serial and parallel concatenated schemes have been studied in [7], [8]. In EXIT chart, the area under EXIT curve of an inner decoder component is approximately equal to the attainable channel capacity, provided that the channel's input symbols are equiprobable [9].

Against the above-mentioned backgrounds, in this paper we will present some results of computing Differential Discrete-input Continuous-output Memoryless Channel (D-DCMC) capacity of the HAP systems employing the non-coherent detection for fading channels associated with different weather conditions using EXIT chart. These novel contributions of the paper are as follows:

- *We first clarify a framework of the HAP based systems, where we focus on characterizing the fading channel model, where the effects of both fast fading and slow fading are taken into consideration along with different path loss scenarios;*
- *We present the results of calculating the D-DCMC capacity for HAP based systems in clear-sky condition using the EXIT chart;*
- *D-DCMC channel capacity is formulated for benchmarking the design of HAP based systems employing specific differential modulation schemes.*

The rest of the paper is organized as follows. The HAP system model is introduced in Section 2. D-DCMC capacities for HAP is presented in Section 3. Section 4 is used for offering our conclusions.

2. HAP system model

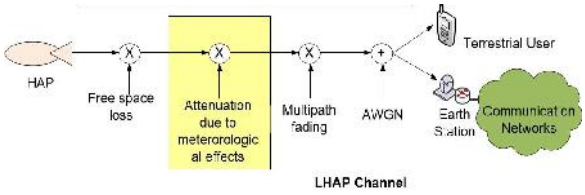

Fig. 2. LHAP channel model.

Our HAP based communication system operating in millimeter wave frequencies is illustrated in Fig. 2, including a HAP, a land high-altitude platform (LHAP) link, and a terrestrial user (both fixed or mobile), where LHAP link is affected by various influences of the propagation environment such as free space loss, attenuation due to meteorological effects, and multipath fading.

Let us now consider a single LHAP link in Fig. 2, associated with the transmitted and received signals of x and y, respectively. The received signal can be represented as

$$y = hx + n, \quad (1)$$

where $h=Ah_sh_f$ is the complex-valued fading coefficient that comprises three components. The first component is the path loss A that includes free space

loss and attenuations associated with above-mentioned weather scenarios. The second component is the block fading coefficient h_s that is also known as slow fading, large-scale shadow fading or quasi-static fading, which may be deemed to be constant for all symbols within a frame duration. The third component is the fast fading or small-scale fading h_f, which fluctuates on a symbol-by-symbol basis. Finally, n is the AWGN process having a variance of $N_0/2$ per dimension.

Let us now continue to discuss the path loss A pertaining to different weather conditions during the year, namely clear-sky and rainy conditions. Due to the presence of atmospheric oxygen, water vapor attenuation during the clear-sky condition, attenuation in this condition $A_{clear-sky}$ in dB can be expressed as:

$$A_{clear-sky} = A_o + A_w, \quad (2)$$

where A_o is the attenuation due to oxygen and A_w is the attenuation due to water vapor.

During the rainy condition, it is assumed that the effect of atmospheric gases, cloud and rain are fully correlated so that the associated attenuation exceeds with the same probability that happens simultaneously for all the phenomena [10]. Hence, this gives pessimistic values for low outage times, hence this can be used for the worst case approximation. As a result, the total attenuation in the rainy condition A_{RC} can be given by [10]:

$$A_{RC} = A_o + A_w + A_{cloud} + A_{rain}, \quad (3)$$

where A_{cloud} is attenuation due to cloud and A_{rain} is attenuation due to rain.

Considering the frequency of f = 28GHz and f = 30GHz typically used in Asian region, Tab. 1 lists magnitudes of path loss A occurring on the LHAP link, which is subject to the influences of atmospheric gases, cloud, rain. Values of the path loss A may be calculated as follows:

$$A = A_{fs} + A_a, \quad (4)$$

where A_{fs} is the free-space loss and A_a is the atmospheric attenuation due to influences of weather conditions; A_a=A_g in the clear-sky condition or A_a=A_{RC} in the rainy condition.

Table 1. Path loss magnitude of the LHAP link, when measured at an elevation angle of θ=12^0, a temperature of t^0=7^{0}C, the water vapor concentration of ρ=6g/m^3, the absolute humidity of 10g/ m^3 and the average rain density of 0.01%/year [10].

Path loss A (dB)	*f = 28GHz*	*f = 30GHz*
Clear-Sky	157.4020 dB	158.5402 dB
Rainy	200.9416 dB	206.8696 dB

3. HAP's capacity of differential discrete-input continuous-output memoryless channel

3.1 D-DCMC capacity for given differential modulation schemes and beneficial applications

When a fixed modulation scheme is activated in the HAP system, the associated Discrete-input Continuous-output Memoryless Channel (DCMC) capacity may be achieved by invoking an idealized channel coding scheme [11]. Without generality, let us assume that the information transmitted over the channel has uniform distribution. By employing the classic Monte Carlo simulation method for averaging the expectation terms, the DCMC capacity of the transmission link may be calculated by [12]:

$$C_{(\mathcal{A})}^{DCMC}(R) = \mathcal{A} - \frac{1}{L}\sum_{l=1}^{L} E\left[\log_2 \sum_{z=1}^{L} \exp\left(\gamma_{l,z}\right)\Big|_{X_l}\right] \text{ [BPS]}, \quad (5)$$

where $L = 2^{\eta}$ is the number of modulation levels, while η is the number of modulated bits and $E\left[A \middle| X_l\right]$ is the expectation of A conditioned on the L-ary signals X_l. Note that $\gamma_{l,z}$ is a function of both the transmitted signal and of the channel as defined in [12]. For the system relying on a single transmit and a single receiver antenna, we have

$$\gamma_{l,z} = \frac{-\left|h\left(x_l - x_z\right) + n\right|^2 + \left|n\right|^2}{N_0}. \quad (6)$$

We define ratio of the power transmitted from the transmitter to the noise power encountered at the receiver [13] as $SNR_t = E\left[\frac{1}{|h|^2} SNR_r\right]$. At a given throughput R, we readily identify the corresponding signal to noise power ratio $SNR_t\big|_R$ that is defined as the SNR value associated with the capacity on the capacity curve, where a throughput of R may be maintained.

Let us now consider the DCMC capacity of differentially encoded schemes D-DCMC, having a throughput R given by

$$R = \kappa R_c, \tag{7}$$

where κ is the number of modulated bits and R_c is the equivalent channel coding rate.

In contrast to the DCMC capacity, where the maximum rate expression was given in Eq. (5), we invoke EXIT charts for calculating the D-DCMC channel capacity supported by the non-coherent detection scheme. For example, the area under the EXIT curve of Differential Quadrature Phase Shift Keying (DQPSK) modem quantifies its attainable capacity. Accordingly, in order to obtain the capacity curves seen in Fig. 3, we employed iteratively decoded system at the receiver including multiple-symbol differential detection (MSDD) de-mapper and unity rate coded (URC) decoder, and carried out the following steps:

- Firstly, we generate the EXIT curves of various differential modulation schemes (e.g. DQPSK) for different SNR_t values.
- Then, we determine a single point on the capacity curves (C) by computing the area under an EXIT curve and its corresponding SNR_t is given by [14]

$$C = A_i\left(SNR_t\right) = \int_0^1 T_i\left(i, SNR_t\right) di, \tag{8}$$

where $A_i\left(SNR_t\right)$ is area under the EXIT curves of various differential modulation schemes at a particular SNR_t value; $T_i\left(i, SNR_t\right)$ is a evaluated EXIT curve at SNR_t value. As a result, the capacity curves are plotted in Fig. 3 for an uncorrelated Rayleigh fading channel, when employing Differential Binary Phase Shift Keying (DBPSK) and DQPSK modulation schemes for HAP based systems on clear-sky condition.

As an alternative method, we also can obtain the D-DCMC capacity curves by shifting the corresponding DCMC capacity curves plotted in Figure 3 [15] to the right by 3dB. As a result the D-DCMC curves determined by the shifting method are also plotted in Fig. 3.

Having plotted the D-DCMC capacity curves, at a given throughput of R, we can now specify the $SNR_t^{EXIT}|_R$ required for maintaining this specific throughput, again as seen in Fig. 3. In our forthcoming discourse, we will opt for using the D-DCMC capacity curve determined by the EXIT-chart based procedure. As a result, the required values of $SNR_t^{EXIT}|_R$ are listed in Tab. 2 for different values of the normalized throughput $R_n = R/\kappa$.

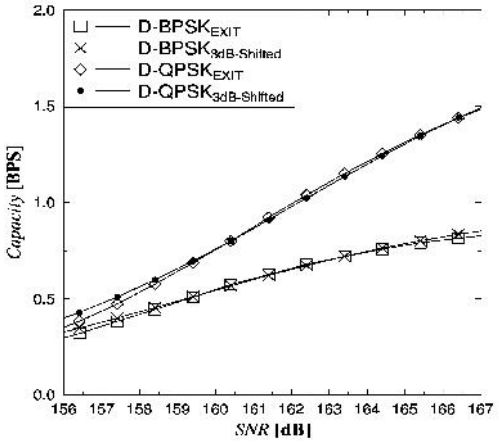

Fig. 3. Capacity curves of the D-DCMC determined by the EXIT chart based method or by shifting for HAP based systems in clear-sky condition.

Table 2. Values of $SNR_t^{EXIT}|_{R_n}$ calculated with the aid of the EXIT charts for a D-DCMC scheme, when various normalized throughput R_n are considered.

Normalized throughput	$SNR_t^{EXIT}\|_{R_n}$ [dB]	
$R_n = R/\kappa$	**DBPSK** (κ = 1)	**DQPSK** (κ = 2)
0.01	145.372	147.092
0.20	154.272	156.622
0.80	165.292	168.722
0.99	185.402	189.402

Then, upon replacing $SNR_t|_R$ of Eq. (16) [15] by $SNR_t^{EXIT}|_R$, the outage probability of the D-DCMC mode for the uncorrelated Rayleigh (fast) and the block Rayleigh (slow) fading channels can also be formulated as follows:

$$P_e^{D-DCMC,f}(R,\kappa) = P_r\left\{\frac{1}{\mathrm{E}[|A|^2|h_f|^2]} < \frac{SNR_t^{EXIT}|_R}{SNR_r}\right\} \tag{9}$$

and as:

$$P_e^{D-DCMC,s}(R,\kappa) = P_r\left\{\frac{1}{|A|^2|h_s|^2} < \frac{SNR_t^{EXIT}|_R}{SNR_r}\right\}. \tag{10}$$

Accordingly, by employing Eq. (18) [15] and the $SNR_t^{EXIT}|_R$ values listed in Tab. 2, the resultant

outage probability can be quantified for diverse values of the normalized throughput R_n for the block Rayleigh fading channel for HAP based systems in clear-sky condition, when various differential modulation schemes are employed, as seen in Fig. 4.

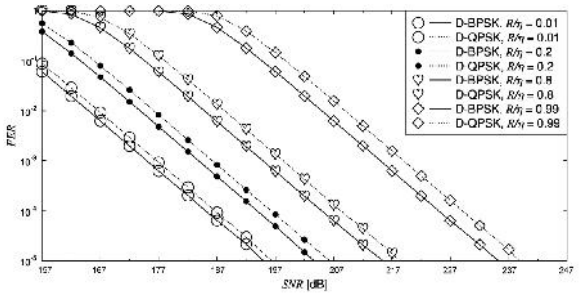

Fig. 4. Outage probability (Frame Error Ratio-FER) of the D-DCMC calculated by Eq. (11) for HAP based systems in clear-sky condition.

3.2. Outage capacity for given modulation schemes and beneficial applications

As noted in [16], channel coding cannot significantly improve the achievable error probability in block fading channels, where the channel coefficients remain constant over the period of a frame. This is because in this specific scenario the channel is an AWGN channel associated with different *SNRs* and the system's performance is dominated by the low-SNR frames. More specifically, in the presence of the small-scale fading, where the channel coefficients change for every symbol, the transmitter can send data at the rate of $R < C|_h$, while maintaining an arbitrarily low error probability. However, it may not be possible to maintain a vanishingly low Bit Error Ratio (BER) for a large-scale fading channel, where the channel coefficients remain constant over a frame duration. Hence, the capacity of large-scale fading channels may become zero in the strict sense.

Alternatively, the outage capacity $C(e)$ introduced in [16] was defined as the highest possible value of transmission rate *R*, which was still capable of ensuring that the outage probability (FER) becomes less than e. It should be noted that the capacity of the quasi-static fading channels is dependent on the outage probability e characterizing the desired quality of transmission. Thus, the outage capacity is different from the capacity represented by Eq. (11) [12].

Similar to the formulaic relationship established for the CCMC case in [16], it can be inferred from Eq. (16) [15] that the outage capacity of the DCMC channel may be formulated as:

$$SNR(e, \mathcal{A}) = F^{-1}(1-e), \tag{11}$$

where $F(SNR_t|_R)$ is the Complementary Cumulative Distribution Function (CCDF) of the combined fast- and slow-fading (small-and large scale-fading) envelope of $|h|^2 = |A|^2 |h_s|^2 |h_f|^2$, which is defined as

$$F(SNR_t|_R) = Pr\left\{\frac{1}{|A|^2|h_s|^2} > \frac{SNR_t|_R}{SNR_r}\right\}. \tag{12}$$

Note that $F(SNR_t|_R)$ depends on the transmission rate R, while the corresponding SNR_t may be calculated from Eq. (11) [12]. In order to provide a fair comparison of the different throughput modulation schemes, the CCDF $F(SNR_t|_{R_n})$ of SNR_t is used at the same value of the normalized transmission rate R_n. Accordingly, Eq. (12) becomes

$$F(SNR_t|_{R_n}) = Pr\left\{\frac{1}{|A|^2|h_s|^2} > \frac{SNR_t|_{R_n}}{SNR}\right\}. \tag{13}$$

In this paper, the uncorrelated Rayleigh fading is chosen for the small-scale fading scenario. Accordingly, each uncorrelated Rayleigh fading coefficient is uncorrelated and varies on symbol-by-symbol basis. By contrast, the block fading is also chosen to be Rayleigh distributed, but each block Rayleigh fading coefficient remains constant during a frame duration and varies independently on frame-by-frame basis.

It should be noted that the general outage capacity formula of Eq. (11) can also be used for the D-DCMC case, where the CCDF $F(SNR_t|_R)$ of the achievable rate R is replaced by $F(SNR_t^{EXIT}|_R)$, which can be defined as

$$F(SNR_t^{EXIT}|_R) = Pr\left\{\frac{1}{|A|^2|h_s|^2} > \frac{SNR_t^{EXIT}|_R}{SNR_r}\right\}. \tag{14}$$

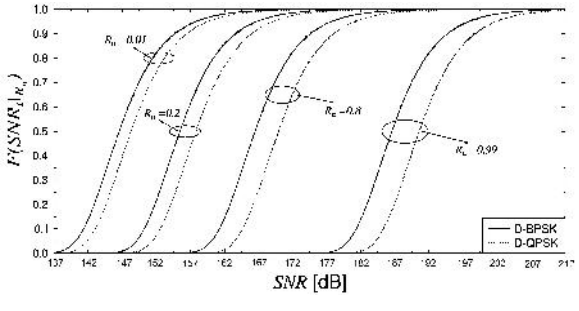

Fig. 5. The CCDF of $F(SNR_t^{EXIT}|_{R_n})$ of Eq. (15).

Note that the CCDF $F(SNR_t^{EXIT}|_R)$ depends both on the transmission rate R and on the

modulation scheme employed. These two parameters allow us to specify the $SNR_t^{EXIT}|_R$ value on the corresponding capacity curve calculated by the EXIT chart based method, as mentioned in Section 3.1, are plotted in Fig. 3. Similarly to the DCMC case in [15], we also employ the normalized transmission rate R_n for the sake of comparing various differential modulation schemes. Hence, Eq. (14) becomes

$$F(SNR_t^{EXIT}|_{R_n}) = Pr\left\{\frac{1}{|A|^2|h_s|^2} > \frac{SNR_t^{EXIT}|_{R_n}}{SNR_r}\right\}, \quad (15)$$

where $SNR_t^{EXIT}|_{R_n}$ is the value corresponding to R_n on the capacity curve. Having calculated $SNR_t^{EXIT}|_{R_n}$, as listed in Tab. 2, the CCDF $F(SNR_t^{EXIT}|_{R_n})$ of Eq. (15) is drawn in Fig. 5 against the SNR and parameterized by different values of the normalized throughput, namely $R_n = 0.01, 0.2, 0.8, 0.99$, for the scenario of employing various differential modulation schemes, when communicating over the block Rayleigh fading channel in HAP based systems in clear-sky condition.

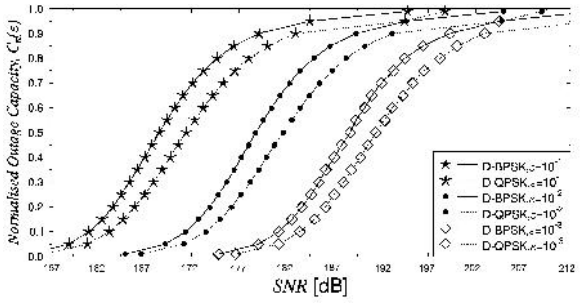

Fig. 6. The normalized outage capacity $C_n(\varepsilon)$ of the D-DCMC for HAP based systems in clear-sky condition.

Then, the CCDF $F(SNR_t^{EXIT}|_R)$ of Eq. (14) or the CCDF $F(SNR_t^{EXIT}|_{R_n})$ of Eq. (15) can be used in conjunction with Eq. (11) for calculating the outage capacity of a perfect D-DCMC capacity-achieving system. For the sake of comparison between various differential modulation schemes, the normalized outage capacity $C_n(\varepsilon)$ defined by $C_n(\varepsilon) = C(\varepsilon)/k$ where $C(\varepsilon)$ is the outage capacity determined by the relationship of Eq. (11), is utilized for characterizing the outage capacity of a perfect D-DCMC capacity-achieving system. As a result, we have Fig. 6 showing the normalized outage capacity pertaining to a range of outage probability values ε, namely to $\varepsilon = 10^{-1}, 10^{-2}$ and 10^{-3}, when the various differential modulation schemes are used for communicating over the block Rayleigh fading channel for HAP based systems in clear-sky condition.

4. Conclusion

In the paper, we have formulated the channels in HAP systems in order to propose the computation of the D-DCMC channel capacity of the HAP systems for fading channels corresponding to various weather conditions using EXIT chart. The D-DCMC channel capacity can be used as the best-possible performance of transmission links in the HAP based systems, when employing specific differential modulation schemes.

References

[1] N. Nomikos, E. T. Michailidis, D. Vouyioukas, and A. Kanatas, "Mobile-to-mobile communications via stratospheric relays: Relay selection and performance analysis," in *2015 IEEE International Conference on Communications (ICC)*, pp. 916–921, IEEE, 2015.

[2] D. Grace and M. Mohorcic, *Broadband Communications via High Altitude Platforms*. John Wiley & Sons, 2011.

[3] M. Alleven, *Google pushes FCC to study high-altitude platform stations for broadband services*, [online] Available at: <http://www.fiercewireless.com/tech/google-pushes-fcc-to-study-high-altitude-platform-stations-for-broadband-services>, [Accessed 25 May 2015]

[4] D. R. Smith, *Digital transmission systems*. Springer science & business media, 2012.

[5] S. S. Haykin, *Modern wireless communications*. Pearson Education India, 2011.

[6] S. Ten Brink, "Convergence behavior of iteratively decoded parallel concatenated codes," *IEEE transactions on communications*, vol. 49, no. 10, pp. 1727–1737, 2001.

[7] A. Grant, "Convergence of non-binary iterative decoding," in *Global Telecommunications Conference*, 2001. GLOBECOM'01. IEEE, vol. 2, pp. 1058–1062, IEEE, 2001.

[8] H. Chen and A. Haimovich, "Exit charts for turbo trellis-coded modulation," *IEEE Communications Letters*, vol. 8, no. 11, pp. 668–670, 2004.

[9] A. Ashikhmin, G. Kramer, and S. ten Brink, "Extrinsic information transfer functions: model and erasure channel properties," *IEEE Transactions on Information Theory*, vol. 50, pp. 2657–2673, Nov. 2004.

[10] S. K. Agrawal and P. Garg, "Calculation of channel capacity considering the effect of different seasons for higher altitude platform system," *Wireless personal communications*, vol. 52, no. 4, pp. 719–733, 2010.

[11] M. C. Valenti and B. Zhao, "Distributed turbo codes: towards the capacity of the relay channel," in *IEEE*

58th Proc. VTC 2003-Fall Vehicular Technology Conference 2003, vol. 1, pp. 322–326, Oct. 6–9, 2003.

[12] S. X. Ng and L. Hanzo, "On the mimo channel capacity of multidimensional signal sets," *IEEE Transactions on Vehicular Technology*, vol. 55, no. 2, pp. 528–536, 2006.

[13] H. Ochiai, P. Mitran, and V. Tarokh, "Design and analysis of collaborative diversity protocols for wireless sensor networks," in *Proc. VTC2004-Fall Vehicular Technology Conference 2004 IEEE 60th*, vol. 7, pp. 4645–4649, Sept. 26–29, 2004.

[14] M. El-Hajjar and L. Hanzo, "Exit charts for system design and analysis," *IEEE Communications Surveys & Tutorials*, vol. 16, no. 1, pp. 127–153, 2014.

[15] Hien Nguyen Thu, Hung Nguyen Viet, Thang le Nhat "Channel capacity of high altitude platform stations employing coherent detection," *Journal of Military Science and Technology*, vol. 46, pp. 36–42, 2016.

[16] D.Tse and P. Viswanath, *Fundamentals of Wireless Communications*. Englewood Cliffs, NJ, USA: Cambridge: Cambridge University Press, 2005.